Optics Communications 285 (2012) 3187–3190

Contents lists available at SciVerse ScienceDirect

Optics Communications

journal homepage: www.elsevier.com/locate/optcom

Defect modes supported by optical lattices in photovoltaic-photorefractive crystals

Kehao Li [a,b], Keqing Lu [a,*], Jianbang Guo [a,b], Weijun Chen [c], Tongtong Sun [c], Fengxue Yao [c], Jingjun Xu [d]

[a] State Key Laboratory of Transient Optics and Photonics, Xi'an Institute of Optics and Precision Mechanics, Chinese Academic of Sciences, Xi'an 710119, China
[b] Graduate School of Chinese Academy of Sciences, Beijing 100039, China
[c] School of Electronics and Information Engineering, Tianjin Polytechnic University, Tianjin 300387, China
[d] Department of Physics, Nankai University, Tianjin 300071, China

ARTICLE INFO

Article history:
Received 22 October 2011
Accepted 2 March 2012
Available online 17 March 2012

Keywords:
Defect modes
Photovoltaic effect
Optical lattices
Nonlinear optics

ABSTRACT

We study defect modes in optically induced one-dimensional lattices in photovoltaic-photorefractive crystals. These defect modes exist in different bandgaps due to the change of defect intensity. For a positive defect, defect mode branches exist not only in the semi-infinite bandgap, but also in the first and second bandgaps. When the defect mode branch is fixed, the confinement of defect modes increases with the defect strength parameter. For a negative defect, defect mode branches exist only in the first and second bandgaps. For a given defect mode branch, the strongest confinement of the defect modes appears when the lattice intensity at the defect site is not the smallest in its branch. On the other hand, when the defect strength parameter is fixed, the most localized defect modes arise in the semi-infinite bandgap for the positive defect and in the first bandgap for the negative defect.

Optical wave propagation in periodic photonic structures has attracted a strong interest because of its fundamental physics and light-routing applications [1,2]. To date, diverse types of self-localized beams in optically induced lattices have been predicted theoretically and observed experimentally in photorefractive crystals, including fundamental [3], multipole [4,5], vortex [6–8], and necklace-like [9] solitons as well as gap soliton trains [10]. It is well known that in a periodic optical medium, linear light propagation exhibits Bloch bands and forbidden bandgaps. If a periodic lattice has a local defect, this defect can support linear localized modes (called defect modes) inside bandgaps of the periodic optical medium. In experiment, reconfigurable optically induced photonic lattices in photorefractive crystals with and without defects were successfully generated [11–13]. This provides an advantage for us to research defect modes in photonic lattices. Thus far, linear defect modes [14–17] and nonlinear defect solitons [18,19] in one-dimensional and two-dimensional photonic lattices have been predicted in biased photorefractive crystals. However, linear defect modes in photonic lattices induced optically in photovoltaic-photorefractive crystals have not yet been explored.

In this article, we analyze defect modes in optically induced one-dimensional lattices in photovoltaic-photorefractive crystals. These defect modes reside in various bandgaps of the photonic lattice. For a positive defect, we find that defect mode branches exist not only in the semi-infinite bandgap, but also in the first and second bandgaps. These defect mode branches occur at the Bloch state on the left edge of each Bloch band and stay inside their respective bandgaps. The confinement of defect modes increases with the defect strength parameter in their branch. For a negative defect, we find also that defect mode branches exist only in the first and second bandgaps. These branches occurring at the Bloch state on the right edge of each Bloch band march to edges of higher Bloch bands and then reappear in higher bandgaps. For a given defect mode branch, the strongest confinement of the defect modes appears when the lattice intensity at the defect site is not the smallest in its branch. We show that when the defect strength parameter is fixed, the most localized defect modes arise in the semi-infinite bandgap for the positive defects and in the first bandgap for the negative defect.

To start, let us consider an ordinarily polarized lattice beam with a single-site defect that propagates in a photovoltaic-photorefractive crystal along the z axis and is allowed to diffract only along the x direction. For illustration purposes, let the photovoltaic-photorefractive crystal be $LiNbO_3$ with its optical c axis oriented along the x direction. Moreover, let us assume that an extraordinarily polarized probe beam with a very low intensity is launched into the defect site, propagating collinearly with the lattice beam. In that case, the nondimensionalized model equation for the probe beam is [14,20]

$$i\frac{\partial U}{\partial Z}+\frac{\partial^2 U}{\partial X^2}+\frac{E_0 I_L(X)}{1+I_L(X)}U=0, \tag{1}$$

where U is the slowly varying amplitude of the probe beam, $E_0=E_p/(\pi^2/T^2k^2n_e^2r_{33})$, E_p is the photovoltaic field constant, T is the lattice spacing, k is the optical wave number in the photovoltaic-photorefractive crystal,

* Corresponding author.
E-mail address: kqlu@opt.cn (K. Lu).

0030-4018/$ – see front matter.
doi:10.1016/j.optcom.2012.03.003

$k=2\pi n_e/\lambda$, λ is the wavelength, n_e is the unperturbed extraordinary index of refraction, r_{33} is the electro-optic coefficient,

$$I_L = I_0 \cos^2(X)[1 + \varepsilon f_D(X)], \tag{2}$$

is the intensity function of the photorefractive lattice, I_0 is the peak intensity of the otherwise uniform photonic lattice, ε controls the strength of the defect, and $f_D(X)$ is a localized function describing the shape of the defect. In obtaining Eq. (1), we have used normalized coordinates, i.e., $Z=z/(2kT^2/\pi^2)$ and $X=x/(T/\pi)$. In this study, let us assume that the defect is restricted to a single lattice site at $X=0$. Thus, we take the defect function $f_D(X)$ as

$$f_D(X) = \exp\left(-X^8/128\right). \tag{3}$$

Other choices of single-site defect functions $f_D(X)$ give similar results. For a positive defect ($\varepsilon>0$), the lattice light intensity I_L at the defect site is higher than that at the surrounding sites. For a negative defect ($\varepsilon<0$), the lattice intensity I_L at the defect site is lower than that at the surrounding sites. The intensity distributions of optical lattices with $\varepsilon=0.5$ and -0.8 are displayed in Figs. 4(e) and 7(m), respectively. In this paper, the $LiNbO_3$ parameters at a wavelength $\lambda=0.5$ μm are taken to be $n_e=2.2$, $r_{33}=30\times10^{-12}$m/V, and $E_p=40$kV/cm. Moreover, we choose $I_0=3$ and $T=20$ μm, which are typical experimental conditions [14]. For this set of values, $E_0\approx18$, one X unit corresponds to 6.4 μm, and one Z unit corresponds to 2.2 mm.

In order to obtain the defect modes in the bandgaps, let us first look at the dispersion relation and bandgap structure of Eq. (1) with $\varepsilon=0$. According to the Bloch theorem, eigenfunctions of Eq. (1) can be sought in the form of

$$U(X, k_X) = u(X)\exp(ik_X X - i\beta Z), \tag{4}$$

where β is the Bloch-wave propagation constant, k_X is wave number in the first Brillouin zone bounded between $-1\le k_X\le1$, $u(X)$ is a periodic function with the same periodicity as the lattices. Substitution of the form of $U(X, k_X)$ into Eq. (1) with $\varepsilon=0$ leads to the following eigenvalue equation

$$\frac{\partial^2 u}{\partial X^2} + 2ik_X\frac{\partial u}{\partial X} - k_X^2 u + V(X)u = -\beta u, \tag{5}$$

with the uniform periodic potential

$$V(X) = \frac{E_0 I_0 \cos^2(X)}{1 + I_0\cos^2(X)}. \tag{6}$$

We calculate Eq. (5) using numerical techniques to obtain the dispersion relation as shown in Fig. 1. It can be seen that there exist three complete gaps which are named the semi-infinite, first, and second gaps respectively. These bandgaps correspond to the white areas in Fig. 1 from the bottom to the top, separated by the shaded Bloch bands.

The defect modes in Eq. (1) are sought in the form $U(X,Z)=u(X)\exp(-i\beta Z)$, where $u(X)$ is a real function and satisfies the linear eigenvalue equation

$$\frac{\partial^2 u}{\partial X^2} + \frac{\partial^2 u}{\partial Y^2} + \frac{E_0 I_L}{1 + I_L}u = -\beta u, \tag{7}$$

from which linear defect modes can be determined by expanding the solution $u(X)$ into discrete Fourier series and then converting Eq. (7) into a matrix eigenvalue problem with β as the eigenvalue [14].

Let us first consider defect modes in Eq. (7) when the defect strength parameter ε varies from -1 to 1. We have obtained the defect modes at each ε value, and the entire diagram of defect eigenvalues versus ε is shown in Fig. 2. For a positive defect ($\varepsilon>0$), a defect mode bifurcates from the left edge of each Bloch band into the bandgap. For a negative defect ($\varepsilon<0$), a defect mode bifurcates from the right edge of each Bloch band into the bandgap. Notice that there are no defect modes in the semi-infinite bandgap when $\varepsilon<0$. Recall that the left and right edges of Bloch bands in Fig. 2 correspond to the lower and upper edges of Bloch bands in Fig. 1, thus Bloch states at circled locations in Fig. 1 and defect modes at the circled points *a*, *b*, *c*, *d* of Fig. 2 are one and the same. Fig. 3 shows the first four Bloch states at the circled points *a*, *b*, *c*, *d* of Fig. 1. Of these four states, the first two are symmetric, and the last two antisymmetric, in *X*. On the other hand, when $|\varepsilon|$ is increased, defect mode branches move away from band edges. When $\varepsilon>0$, these branches stay inside their respective bandgaps. When $\varepsilon<0$, defect mode branches march to edges of higher Bloch bands and then reappear in higher bandgaps. For example, the defect mode branch in the first bandgap reaches the edge of the second Bloch band at $\varepsilon\approx-0.65$ and reappears in the second bandgap when $\varepsilon\approx-0.65$.

Now we examine defect modes on defect mode branches in Fig. 2. For this purpose, we select the representative points from defect mode branches, mark them by circles, and label them by letters in Fig. 2. Figs. 4–7 depict defect mode profiles at these marked points. The letter labels for these defect modes are identical to those for the marked points on defect mode branches in Fig. 2. First, we examine defect modes on defect-mode branches in Fig. 2 when $\varepsilon>0$. When the defect parameter ε is fixed, we look at the confinement of defect modes in different bandgaps. The lattice-field profile for $\varepsilon=0.5$ can be seen in Fig. 4(a). In this case, three defect modes are displayed in Fig. 4. The first one in the semi-infinite bandgap is quite localized and is symmetric in X [see Fig. 4(f)]. The second one in the first bandgap is more confined than the third one in the second bandgap [see Figs. 4(g) and 4(h)]. The defect mode in the first bandgap is antisymmetric in X, while the defect mode in the second bandgap is symmetric in X. When the bandgap is fixed, the defect parameter ε has

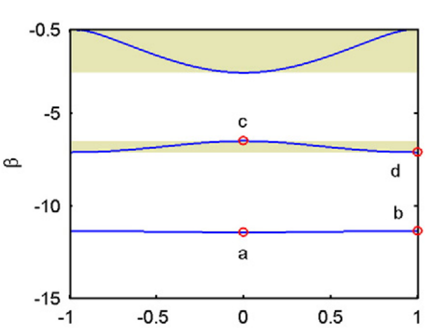

Fig. 1. Dispersion relation of Eq. (5) with $E_0=18$ and $I_0=3$. Shaded: first three Bloch bands. Bloch states at circled locations are displayed in Fig. 3.

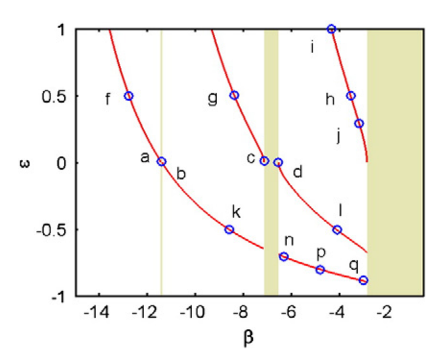

Fig. 2. Bifurcations of defect modes with the defect described by Eq. (2) at $E_0=18$ and $I_0=3$. The shaded regions are the Bloch bands. Profiles of defect modes at the circled points in this figure are displayed in Figs. 3–7.